Journal of Applied Ecology (1983), **20,** 103–115

INSTRUMENTS FOR THE MEASUREMENT OF PHOTOSYNTHETICALLY ACTIVE RADIATION AND RED, FAR-RED AND BLUE LIGHT

By F. I. WOODWARD

Department of Botany, University of Cambridge, Downing Street, Cambridge, CB2 3EA

SUMMARY

(1) The design of an instrument for the simultaneous measurement of photosynthetically active radiation and red, far-red and blue light is described. The optical responses of the instrument closely match the action spectra of photosynthesis and some important photomorphogenic responses within the waveband of 400 to 800 nm.

(2) The design of a single instrument for the measurement of the quantum irradiance at 660 and 730 nm is also shown.

(3) The application of these instruments to measurements in the field and the controlled environment is described.

INTRODUCTION

The photosynthetic and photomorphogenic responses of plants to spectral quality in the 350 to 800 nm waveband have been extensively documented and reviewed (e.g. McCree 1972a, b; Smith 1975; Vince-Prue 1975). All wavelengths of radiation between 350 and 725 nm are photosynthetically effective. Three major wavebands, blue (400–500 nm), red (550–700 nm) and far-red (550–800 nm) are known to have profound photomorphogenic effects. Experiments on the growth and development of plants should include measurements of the irradiance over these defined wavebands. This is necessary when radiation conditions in both the controlled environment and the field need to be compared or standardized.

Precise measurements of red and far-red light, which control the photoconversions of phytochrome (Kendrick & Frankland 1976; Smith 1975), have only been possible, to date, with very expensive spectroradiometers. These instruments scan and record the irradiance over a waveband, typically the visible and near infra-red wavelengths. These instruments have slow response times, a severe disability in the field, where the irradiance may vary rapidly under vegetation or broken cloud. Weighting functions, e.g. the photosynthetic action spectrum, may be applied to the recordings of the spectroradiometer, for the purpose of predicting the plant response, photosynthesis in this case.

A simpler technique for routine experimental work would be the use of an instrument which responds to different wavelengths in the same manner as the plant response. Such a technique has been achieved by Woodward & Yaqub (1979) for the photosynthetic action spectrum of higher plants (McCree 1972b). This instrument has proved useful for the rapid comparison of widely differing radiation conditions. In addition the device may be left in the field to provide a continuous record of photosynthetically active radiation (PAR), when connected to a chart recorder.

Spectroradiometers are sampling devices and can not provide continuous records of irradiance. Changes in irradiance and spectral quality can have very rapid effects on photosynthesis and on other processes such as plant extension (Gaba & Black 1979:

0021-8901/83/0400–0103 $02.00

Morgan & Smith 1978). So it may be most important to consider the continuous changes in irradiance and spectral quality when analysing plant growth and development. The instruments described in this paper have been designed to respond to spectral quality in the same manner as important photobiological responses. The devices will therefore, be particularly suitable for continuous recording and predicting the effectiveness of differing radiation environments, both in the field and the controlled environment, for plant growth and development and photosynthesis.

INSTRUMENT DESIGN AND CONSTRUCTION

The optical responses of the instruments must be defined in terms of known, important photobiological responses. Plant growth and development is controlled by radiation in the waveband between about 350 and 800 nm and four pigment systems may be recognized throughout the plant kingdom, both by their action spectra and subsequent plant responses. A search through published action spectra indicates that the response curves of different species are similar. Four responses have been selected and these include photosynthesis (Fig. 1(a) from McCree 1972a), the blue light response (Fig. 2(a) from

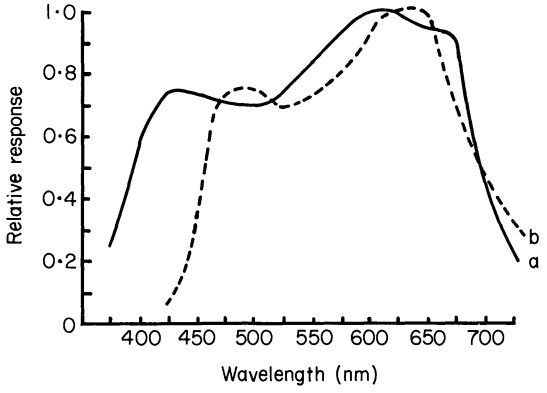

FIG. 1. (a) Relative quantum yield of photosynthesis (from McCree 1972a). (b) Relative quantum response curve of the photocell for photosynthetically active radiation.

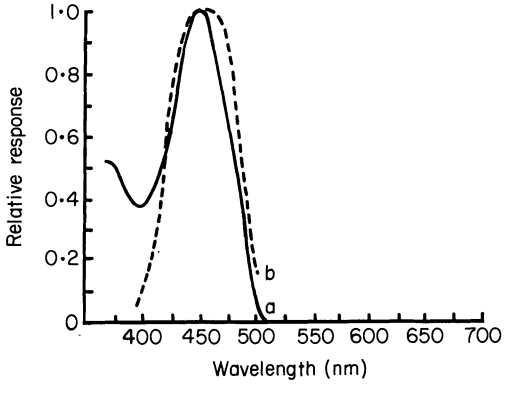

FIG. 2. (a) Relative quantum yield for phototropism in the *Avena* coleoptile (from Everett & Thimann 1968). (b) Relative quantum response curve of the photocell for blue light.

Everett & Thimann 1968), the red light response (Fig. 3(a) from Toole *et al.* 1956) and the far-red light response (at wavelengths greater than 500 nm in Fig. 4(a) from Mohr 1959). The action of phytochrome in both the red and far-red light responses is well documented and its action spectra are shown in Fig. 5(a) (from Butler, Hendricks & Siegelman 1964).

The design of two instruments is presented here. One instrument, the multisensor, is capable of simultaneous measurements of PAR, red light, far-red light and blue light. The optical responses of the multisensor have been tailored to the photobiological responses mentioned above. The actual response curves are shown on Figs 1(b) to 5(b), with the associated plant responses. The optical responses of the multisensor are closely correlated with known photobiological responses. However, at present, most research workers in photomorphogenesis who are concerned with measurements of red and far-red radiation, just measure the quantum irradiance at two wavelengths, 660 ± 5 nm (red light) and 730 ± 5 nm (far-red light). This is a simple objective technique but it is clearly inadequate for accounting for the wideband response of phytochrome (Fig. 5(a)). An instrument with this response has been used to assess the responses of the multisensor. The response curves of the second instrument are shown on Fig. 6.

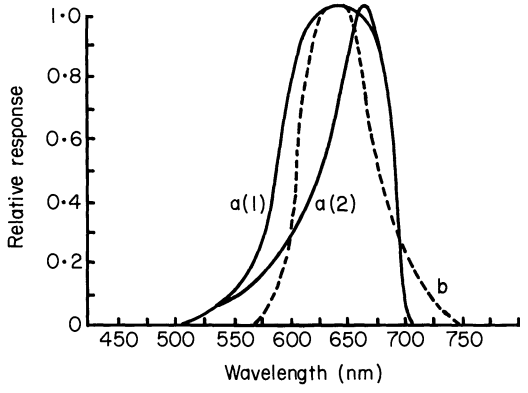

FIG. 3. (a) Relative quantum yields for the promotion of seed germination in *Lactuca sativa* (1) and *Lepidium sativum* (2) (from Toole *et al.* 1956). (b) Relative quantum response curve of the photocell for red light.

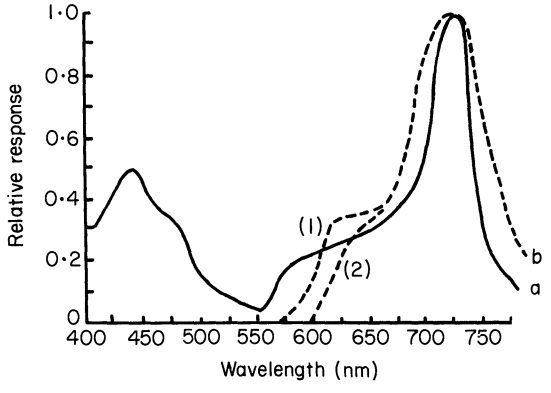

FIG. 4. (a) Relative quantum yield for the expansion of cotyledons of *Sinapis alba* (from Mohr 1959). (b) Relative quantum response curves of the photocell for far-red light with an RG610 filter (1) or an RG630 filter (2).

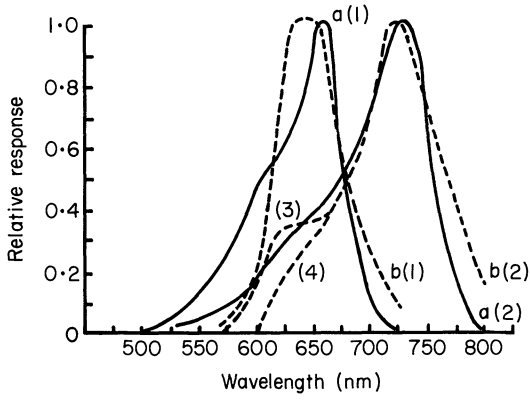

FIG. 5. (a) Relative quantum yields for the *in vitro* photoconversion of phytochrome Pr (1) and Pfr (2) (from Butler *et al.* 1964). (b) Relative quantum response curves for the photocell for red light (1) and far-red light (2), with an RG610 filter (3) or an RG630 filter (4).

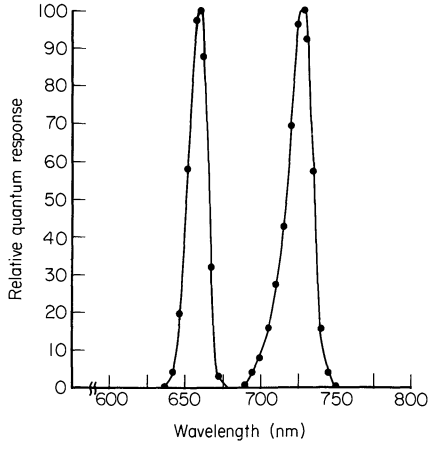

FIG. 6. Relative quantum response curves for the 660 : 730 nm detector.

Both of the instruments use a sensitive photocell plus amplifier combination as the radiation detector (see Appendix). The response curve of the photocell is modified by optical filters to provide the response curves shown in Figs 1–6. The appropriate filter combinations are shown in Table 1.

The cosine-corrected heads of the two instruments are shown in longitudinal section, in Figs 7 and 8. The cosine-corrected heads are constructed from black acetal polymer (Delrin) rod. The rod for the multisensor was sliced at an angle of 45° into two parts, along the line 1 to 2 (Fig. 7), with a milling machine. The upper surface of the top section was cut to provide a cosine-corrected response (Biggs *et al.* 1971). A 15 mm diameter diffusing disc (A) was constructed from white acetal polymer (Delrin) and was 3 mm thick.

The incident radiant flux passes through the diffuser and through two, 15 mm diameter Schott KG3 heat-absorbing glass filters (B1 and B2 in Fig. 7). These filters transmit radiation between 350 and 600 nm and are increasingly opaque to longer wavelengths, so that virtually no radiation is transmitted beyond approximately 825 nm. The radiation

TABLE 1(a). Filter combinations for the multisensor

Response	Schott Filter	Strand Filter	Kodak Filter
Blue	BG12		
Red	RG630 + KG3		No. 96 (ND 0·3)
Far-red	RG610 or RG630	No. 21	
PAR	KG1	Nos. 36, 38, 73	CC20C + CC30M

(b) Filters for the 660:730 detector

Response	Interference filter (centre wavelength and code)
660	660 nm, SS-6600-1
730	730 nm, SS-7300-1

Addresses of the suppliers in the appendix.

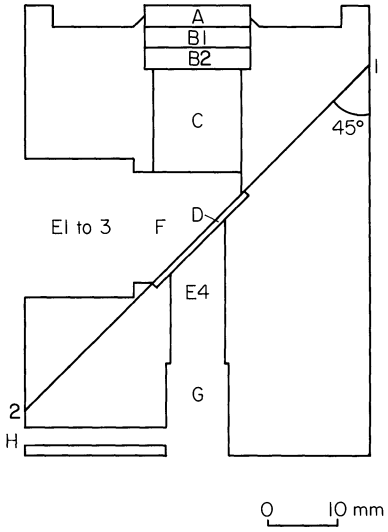

FIG. 7. Section through the cosine-corrected head of the multisensor: A, white Delrin diffuser (15 mm diameter); B1 and B2, Schott glass filters (15 mm diameter); C, 12·5 mm diameter hole filled with acrylic polymer optical fibres, each 1 mm in diameter and excluding the sheath; D, CM1 cold mirror, cut to a 20 mm square; E1–E4, positions of the four photocells.

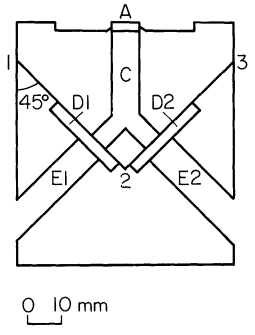

FIG. 8. Section through the cosine-corrected head of the 660:730 detector: A, white Delrin diffuser (8 mm diameter); C, 8 mm diameter hole filled with acrylic polymer optical fibres, each 1 mm in diameter and excluding the sheath; D1 and D2, two Corion interference filters (25·4 mm diameter); E1 and E2, positions of the two photocells.

transmitted through the two KG3 filters was collimated by transmission through 15 mm lengths of 1 mm diameter acrylic polymer optical fibres. The fibres are available with a black plastic sheath. The sheath is removed before insertion to position C.

The lower part of the head was milled to provide a 20 mm wide and 2 mm deep slot, running from point 1 to 2 (Fig. 7) and centred along the largest diameter of the elliptical surface of the head. A cold mirror (see Appendix) was inserted in this slot at position D (Fig. 7). The cold mirror was supplied as a 2 mm thick, 50 mm diameter disc. The mirror was cut with a diamond glass cutter, to provide a 20 mm square. The square was then glued into the central position of the milled slot, ensuring that hole E4 (Fig. 7) was completely covered.

The optical responses of the photocells were modified with the filter combinations shown on Table 1. The Strand and Kodak filters were cut to a diameter of 8 mm, with a sharp cork-borer and were then glued to the glass windows of the photocells with cyanoacrylate adhesive. The 8 mm diameter Schott glass filters were then glued onto the photocells with the same adhesive. The photocell with filters for the far-red response was inserted into hole G and to position E4, which is on the optical centre of the head and beneath the cold mirror. The cold mirror transmits far-red radiation and reflects radiation of shorter wavelengths to the remaining three photocell plus filter combinations at positions E1 to E3 and against the rim of hole F. The glass windows of the photocells face the cold mirror. Each photocell has four electrical leads. These were brought out through hole H for the far-red detector and from the back of the hole with the other three sensors. The holes behind the photocells were filled with a mixture of epoxy glue and black paint. The two parts of the multisensor head were screwed together.

The design of the head of the instrument for measuring radiation at 660 and 730 nm (660:730 detector) is shown in Fig. 8. The head was made from the same material as the multisensor. The rod was cut into two sections using a milling machine. One cut was made between points 1 and 2 (Fig. 8), at an angle of 45°. A second cut was made between points 3 and 2. These two cuts divided the rod into two sections. The surface of the top section was cut to provide cosine-correction. An 8 mm diameter hole was drilled from the surface to a depth of 28 mm (C in Fig. 8). The diffuser (A) is an 8 mm disc of 3 mm thick white acetal polymer. The hole C (Fig. 8) bifurcates to two holes of 6 mm diameter. The centres of these holes are 13 mm from point 2. The incident radiation passes through the diffuser (A) and is then transmitted through 30 mm lengths of 1 mm diameter acrylic polymer optical fibres. The black sheaths of the fibres were removed prior to insertion into position C. Half of the fibres pass through the limb of C to D1 (Fig. 8) and half to D2.

The lower part of the head was drilled to provide locating holes for two photocells (see Appendix), at positions E1 and E2. Two holes with diameters of 25·4 mm and depth 3·5 mm were drilled at position D1 and D2. The 660 and 730 nm interference filters were then inserted into these holes. The two parts of the 660:730 detector head were screwed together.

The electronic circuit associated with each photocell is simple and may be easily modified to suit individual requirements. The circuit for one photocell is shown in Fig. 9. The photocell requires a + and − power supply, to a maximum of ±18 V. A ±5 V supply has been used successfully. The output voltage of the photocell goes negative with increasing irradiance and has an appreciable dark voltage, in the range of 10–40 mV. The circuit shown on Fig. 9 provides a means of offsetting the dark voltage, inverting the negative going output to a positive going signal and can provide additional amplification.

Amplification is set by increasing the resistance of the trimmer (F). The offset voltage is

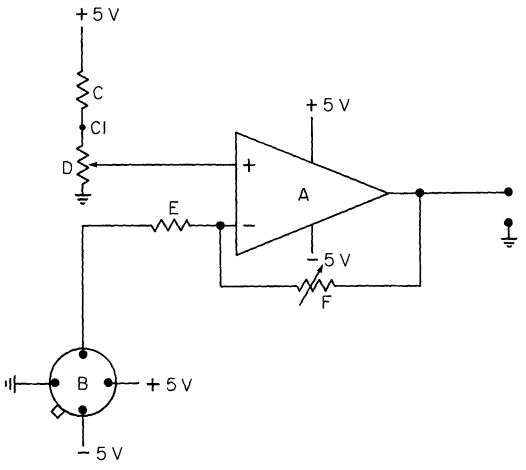

FIG. 9. Electronic circuit for one photocell: A, one of four operational amplifiers in the LM324N integrated circuit; B, the Centronic OSI-5K photocell; C. 1·2 MΩ resistor which should provide approximately 40 mV at point C1; D, 10-turn, 10 KΩ potentiometer; E, 1·2 KΩ resistor; F, 20-turn 10 kΩ cermet trimmer.

derived from the +5 V power supply. The potentiometer D is used to adjust the output voltage of the operational amplifier (A) to 0 V, when the photocell is darkened. Four operational amplifiers are provided in one LM324N integrated circuit, which is sufficient for the analogue conditioning of the multisensor. The output voltage from each amplifier may be switched in turn to a digital millivoltmeter, or the four outputs may be connected to four inputs of a data logger or multi-pen chart recorder. Ratios, for example the red to far-red ratio, may be as a direct readout by using a digital panel meter in the ratiometric mode.

The spectral responses of the instruments were tested between 350 and 950 nm with a monochromator, which was a modified Hilger and Watts H700 spectrophotometer, (wavelength accuracy ±9 nm) with a high pressure Xenon lamp source (Wotan XBO450W). The response of the 660:730 detector was tested with a Pye Unicam SP6-500 UV Spectrophotometer (wavelength accuracy ±1 nm). Each instrument was calibrated in terms of quantum irradiance, in the manner described by Biggs *et al.* (1971), using a standard light source (ISCO model SRC Spectroradiometer calibrator).

RESULTS AND DISCUSSION

The quantum responses shown in Figs 1–5 all demonstrate a very close agreement between the physiological and instrument responses. The poorest agreement is for PAR and is due to insufficient response of the photocell at wavelengths less than 450 nm.

In some cases it is likely that the plant response curves may vary between individuals or species (e.g. Fig. 3(a) and McCree 1972a) so exact matching of instrument and plant response will not always be possible. The errors involved will clearly depend on the light source, the plant response and the magnitude of the difference although most cases show similar qualitative responses, which will allow the use of the instrument without significant problems. The responses of the photocells may be modified by changing the filter selections. For example the far-red response may be modified between 575 and 650 nm by selecting either an RG610 or an RG630 Schott glass filter (Fig. 4(b)).

The cosine responses of both instruments and all photocells showed no significant deviation from a true cosine response up to a zenith angle of 80°.

The output voltages of the instruments were linearly related to irradiance to at least 2000 μE m^{-2} s^{-1} for PAR, 1200 μE m^{-2} s^{-1} for red light, 1300 μE m^{-2} s^{-1} for far-red light and 700 μE m^{-2} s^{-1} for blue light. The amplification provided by the operational amplifiers in Fig. 9 may be adjusted so that each photocell has a simple calibration factor, 1 mV/μE m^{-1} s^{-1} has proved to be satisfactory.

The application of the instruments to measurements in field and controlled environment conditions is demonstrated in Figs 10–15. The red to far-red ratio of the multisensor and the 660:730 detector are compared on Fig. 10(a) for natural radiation and for artificial light sources. It may be seen that the greatest deviation between the two instruments occurs under the far-red deficient fluorescent light source. This emphasizes the difference between the wideband response curve of the multisensor (and of plants), with a far-red response into the higher irradiance waveband of the light source, and the virtually monochromatic response of the 730 nm detector. The differences between the other light sources are much smaller.

The same range of light sources have also been analysed for the ratio between PAR and blue light. The relationships in all cases are linear and with blue light increasing from 8% of PAR, for tungsten light to 36·5% of PAR for sunlight. Only the Wotan metal-halide plus Dysprosium light source has a comparable blue/PAR ratio to sunlight (34·5%), all of the other light sources being deficient in blue light. The apparently high ratio of blue light to PAR is because of the wide waveband of the blue detector (Fig. 2(b)).

The major problem with the multisensor is the poor sensitivity of the PAR detector below 450 nm, the waveband 400–450 nm accounting for up to 10% of PAR in sunlight and as little as about 1% under tungsten lights. The error increases under a mixture of tungsten and fluorescent lights to about 14% because of the high irradiance mercury emission lines in the blue waveband. These errors will remain constant for a particular light

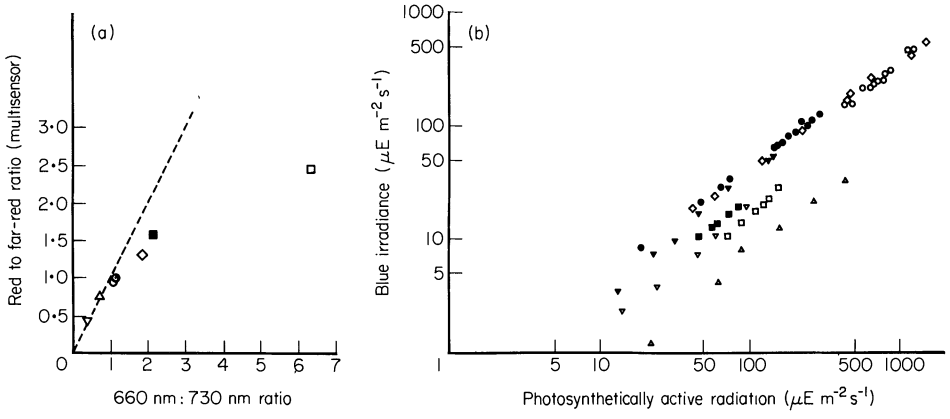

FIG. 10. Instrument responses under different light sources. (a) Comparison of the red to far-red ratio (multisensor) with the ratio of the irradiance at 660 nm to that at 730 nm. (b) Relationship between blue light and photosynthetically active radiation (PAR): (○) outdoor cloudless: (●) outdoor cloudy; (□) fluorescent light (warm-white); (■) warm-white fluorescent plus tungsten lights (ratio of electrical power 2:1); (◇) Wotan metal-halide with Dysprosium additive light (400 and 1000 W); (△) tungsten light (100 W); (▽) Cinemoid No. 21 filter (pea green), natural radiation; (▼) natural shade.

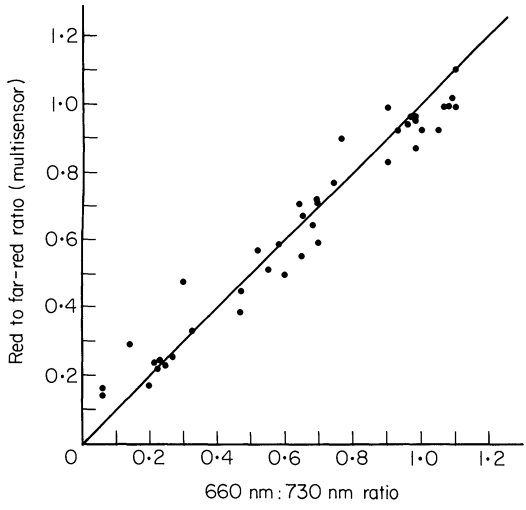

FIG. 11. Comparison between the red to far-red ratio (multisensor) and the 660:730 nm ratio (660:730 detector), under diffuse and direct radiation and shade, in the field.

source and could be predicted from the slopes of the regression lines of blue light upon PAR (Fig. 10(b)).

The relationship between the red to far-red ratio, determined with the multisensor and the 660:730 nm ratio has been assessed under natural illumination, including leaf-shade and is shown on Fig. 11. For reference, the line of the 1:1 relationship has been drawn and a very close relationship between the two techniques of measurement is apparent. The two instruments were placed side by side, under full sunlight and under vegetation and so some of the scatter about the line is due to spatial variation of the red to far-red ratio. The slope of the fitted line is 0·90 and is not significantly different from unity, at a probability of 95%.

The outputs from the red and far-red light detectors may be connected to an analogue divider. The divider provides a voltage output which is linearly related to the red to far-red ratio by a single calibration factor. This voltage may be recorded on a chart recorder to provide a continuous record of the red to far-red ratio. The 660:730 detector has been used in this way above a plant canopy and is shown on Fig. 12, for a period of intermittent cloud cover. It may be seen that the 660:730 nm ratio is more or less unchanging around a mean value of about 1·1. The multisensor was placed at the base of a canopy of *Corylus avellana*, during a period of sunlight. The rapid variations of the red to far-red ratio on the right-hand side of the diagram are due to the effects of leaf flutter, when only one leaf layer was intercepting the solar beam. The red to far-red ratio was less variable when more than one leaf layer intercepted the solar beam.

The rapidity of readout of the instruments and their small size makes this a useful survey instrument. Figure 13 is a plot of PAR against the red to far-red ratio and has been achieved under a range of plant canopies, including both sunflecks and shade radiation. There is a clear logarithmic relationship between PAR and the red to far-red ratio (obtained with the multisensor). It is interesting to note that the red to far-red ratio is greatest under coniferous canopies, with thick leaves acting more like neutral density filters and least under the thin-leaved herbaceous canopies.

The relationships between leaf area density, leaf area index and PAR, blue light, the red

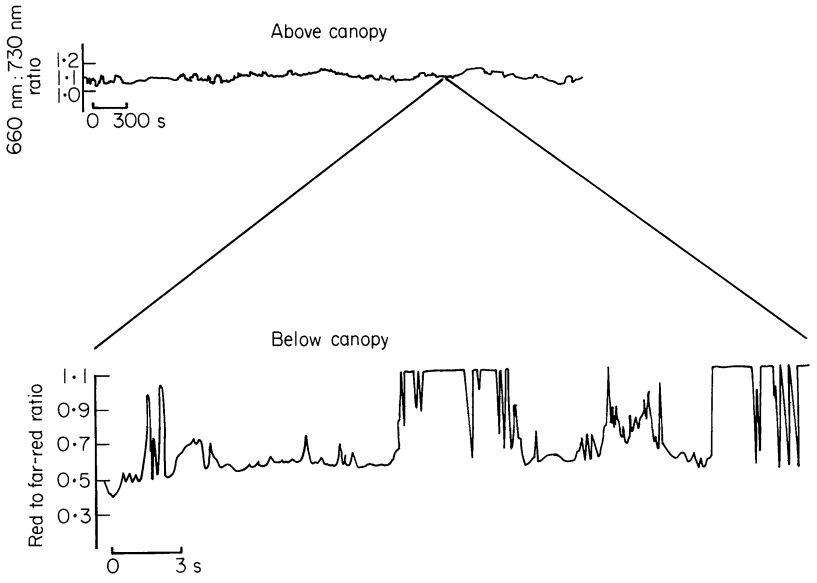

FIG. 12. Temporal changes in the 660:730 nm ratio above and the red to far-red ratio (multisensor) below a canopy of *Corylus avellana*.

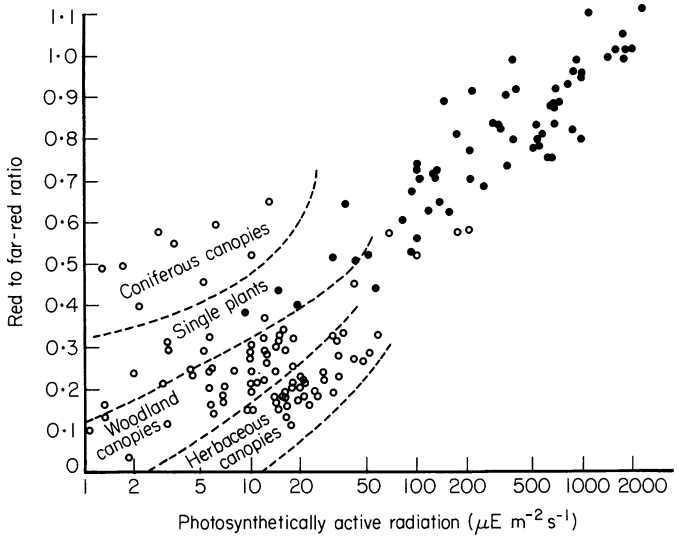

FIG. 13. The relationships between photosynthetically active radiation (PAR) and the red to far-red ratio (multisensor), under different plant canopies. (●) sunflecks; (○) shade radiation.

to far-red ratio (multisensor) and the 660 to 730 nm ratio (660:730 detector), for both shade radiation and sunflecks are shown on Fig. 14, for a canopy of *Buddleia davidii*. There is a clear, exponential decline of both the PAR and blue light content of the shade radiation, correlating with the greatest leaf area density. The change in the two measurements of the red to far-red ratio is less marked, in this rather thin canopy. The changes in spectral quality and quantity are rather small in sunflecks, with no clear relationships with canopy structure.

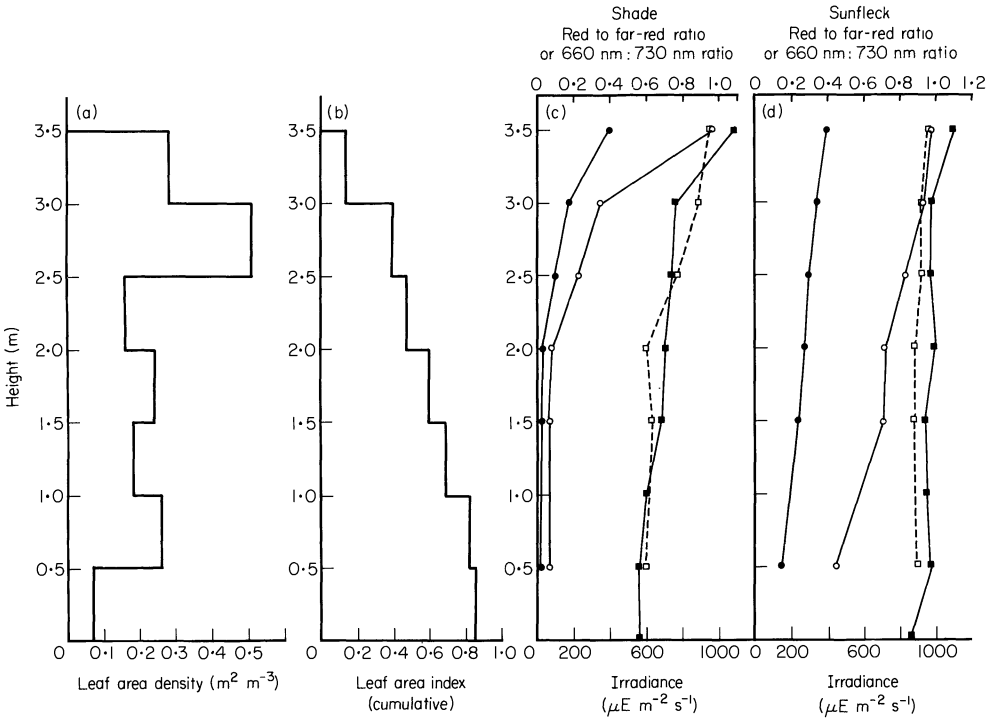

FIG. 14. Relationships between leaf distribution and irradiance in a canopy of *Buddleia davidii*: (a) leaf area density and plant height; (b) cumulative leaf area index and plant height. Photosynthetically active radiation (○); blue light (●); red to far-red ratio (□) (multisensor) and 660 : 730 nm ratio (■); in shade radiation c, and sunflecks d, at different heights.

Remote sensing of vegetation is an increasingly popular area of plant ecology. The important requirement of the technique is the establishment of a relationship between the biomass of the vegetation and some remote, perhaps optical measurement. Figure 12 has indicated that there is likely to be some relationship between leaf biomass and the red to far-red ratio beneath a canopy. However remote sensing would require measurements above the canopy. The application of the multisensor to remote sensing has been tested with canopies of *Trifolium repens* and *Lolium perenne*, which were grown in a controlled environment.

The relationship between the red to far-red ratio at the base of the canopy, and leaf area index or above-ground dry weight is shown in Fig. 15(a). The relationships differ between the species, although only at leaf area indices greater than 4 and an above-ground dry weight of greater than about 100 g m^{-2}. The relationship between the red to far-red ratio and biomass is close to linear below these values. These results suggest a non-destructive technique for estimating above-ground biomass and warrants further investigation. Figure 15(b) also indicates a logarithmic relationship between the penetration of PAR through the canopy and the red to far-red ratio and is in agreement with the results shown in Fig. 13.

The reflected red to far-red ratio was also measured above the plant canopies, viewing the canopy at an angle of 30° from the vertical. This angle is close to the angle of 32·5° proposed by Warren Wilson (1960), for estimating leaf area index with the point quadrat but minimizing the influence of leaf angle on the estimate. The relationship between the reflected and the transmitted red to far-red ratios are shown in Fig. 15(b). It may be seen

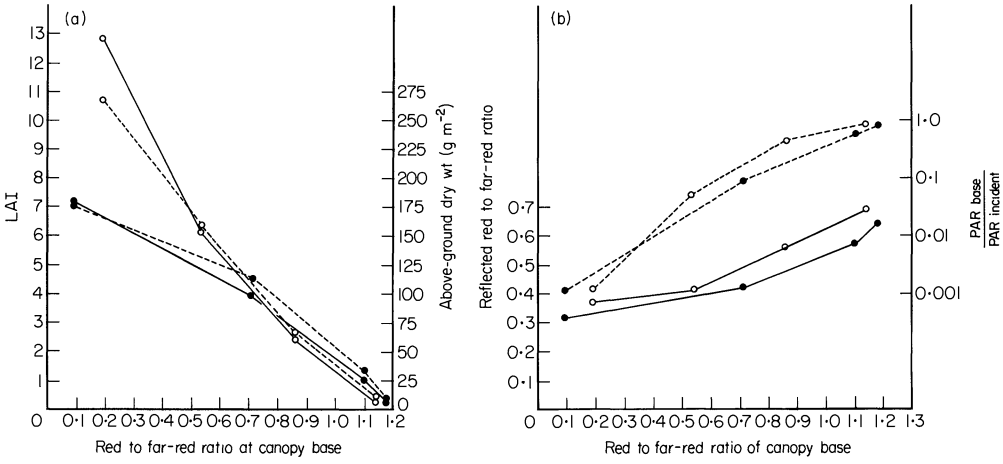

FIG. 15. (a) Relationships between leaf area index (——) and above ground biomass (– – – –) and the red to far-red ratio at the base of canopies of *Lolium perenne* (○) and *Trifolium repens* (●). (b) Relationships between the reflected red to far-red ratio (——) and the penetration of photosynthetically active radiation (PAR) (– – – –) and the red to far-red ratio at the base of *L. perenne* and *T. repens*, (symbols as in (a)).

that there is an approximately linear relationship between the two measurements. Deductions from Fig. 15(a) suggest a linear relationship with leaf area index to about 5 and with above-ground dry weight to about 100 g m^{-2}. The technique is insensitive to greater values. Small but consistent interspecific differences were observed and further studies would be required for further assessments of the potential of this technique in remote sensing.

The two instruments described in this paper have proved to be simple to use both for survey devices at remote sites and for continuous recording with data loggers and chart devices. Testing in the field and the controlled environment has demonstrated that the design criteria of the instruments are well satisfied in practice.

ACKNOWLEDGMENTS

Thanks are due to Mr R. B. Ward for constructing and suggesting improvements to the cosine-corrected heads and to Mr J. Harbinson and Mr P. Freeman for assistance with calibration. I am grateful to Dr J. E. Sheehy for suggesting improvements to the manuscript.

REFERENCES

Biggs, W. W., Edison, A. R., Eastin, J. D., Brown, K. W., Maranville, J. W. & Clegg, M. D. (1971). Photosynthesis light sensor and meter. *Ecology*, **52,** 125–131.

Butler, W. L., Hendricks, S. B. & Siegelman, H. W. (1964). Action spectra of phytochrome in vitro. *Phytochemistry and Photobiology*, **3,** 521–528.

Everett, M. & Thimann, K. V. (1968). Second positive phototropism in the *Avena* coleoptile. *Plant Physiology*, **43,** 1786–1792.

Gaba, V. & Black, M. (1979). Two separate photoreceptors control hypocotyl growth in green seedlings. *Nature*, **278,** 51–54.

Kendrick, R. E. & Frankland, B. (1976). *Phytochrome and Plant Growth.* Institute of Biology. Studies in Biology No. 68. Edward Arnold. London.

McCree, K. J. (1972a). The action spectrum, absorptance and quantum yields of photosynthesis in crop plants. *Agricultural Meteorology*, **9,** 191–216.

McCree, K. J. (1972b). Test of current definitions of photosynthetically active radiation against leaf photosynthesis data. *Agricultural Meteorology*, **10,** 443–453.

Mohr, H. (1979). Der Lichteinfluss auf das Wachstum der Keimblatter bei *Sinapis alba L. Planta*, **53,** 219–245.

Morgan, D. C. & Smith, H. (1978). Simulated sunflecks have large, rapid effects on plant stem extension. *Nature*, **273,** 534–536.

Smith, H. (1975). *Phytochrome and Photomorphogenesis. An Introduction to the Photocontrol of Plant Development*. McGraw-Hill, London.

Toole, E. H., Hendricks, S. R., Borthwick, H. A. & Toole, V. K. (1956). Physiology of seed germination. *Annual Review of Plant Physiology*, **7,** 299–324.

Vince-Prue, D. (1975). *Photoperiodism in Plants*. McGraw-Hill, London.

Warren Wilson, J. (1960). Inclined point quadrats. *New Phytologist*, **59,** 1–8.

Woodward, F. I. & Yaqub, M. (1979). Integrator and sensors for measuring photosynthetically active radiation and temperature in the field. *Journal of Applied Ecology*, **16,** 545–552.

(*Received 12 March 1982; revision received 1 September, 1982*)

APPENDIX

Suppliers of optical filters

(1) Type CM1 cold mirror (50 mm diameter): Barr and Stroud Ltd, Caxton Street, Anniesland, Glasgow, G13 1HZ, Scotland.

(2) Corion interference filters (25·4 mm diameter): Laser Lines Ltd, 19 West Bar, Banbury, Oxfordshire, OX16 9SA, England.

(3) Kodak Colour Compensation Filters: Kodak Ltd, Hemel Hempstead, Hertfordshire, England.

(4) Schott Glass Filters (cut to 8 mm or 15 mm diameters): Precision Optical Instruments (Fulham) Ltd, 158 Fulham Palace Road, London W6, England.

(5) Strand Cinemoid Filters: Rank Strand Electric, P.O. Box 70, Great West Road, Brentford, Middlesex, TW8 9HR, England.

Supplier of photocells

(6) Photocell Type 0SI–5K: Centronic, Centronic House, King Henry's Drive, New Addington, Croydon, CR9 0BG, England.